Digital Baseband Predistortion Based Linearized Broadband Inverse Class-E Power Amplifier

Mury Thian, Ming Xiao, *Student Member, IEEE*, and Peter Gardner, *Senior Member, IEEE*

***Abstract*—A newly introduced inverse class-E power amplifier (PA) was designed, simulated, fabricated, and characterized. The PA operated at 2.26 GHz and delivered 20.4-dBm output power with peak drain efficiency (DE) of 65% and power gain of 12 dB. Broadband performance was achieved across a 300-MHz bandwidth with DE of better than 50% and 1-dB output-power flatness. The concept of enhanced injection predistortion with a capability to selectively suppress unwanted sub-frequency components and hence suitable for memory effects minimization is described coupled with a new technique that facilitates an accurate measurement of the phase of the third-order intermodulation (IM3) products. A robust iterative computational algorithm proposed in this paper dispenses with the need for manual tuning of amplitude and phase of the IM3 injected signals as commonly employed in the previous publications. The constructed inverse class-E PA was subjected to a nonconstant envelope 16 quadrature amplitude modulation signal and was linearized using combined lookup table (LUT) and enhanced injection technique from which superior properties from each technique can be simultaneously adopted. The proposed method resulted in 0.7% measured error vector magnitude (in rms) and 34-dB adjacent channel leakage power ratio improvement, which was 10 dB better than that achieved using the LUT predistortion alone.**

***Index Terms*—Class E, injection, linearization, lookup table (LUT), memory effects, power amplifier (PA), predistortion.**

I. Introduction

THE CLASS-E power amplifier (PA) first introduced by Sokal can offer high efficiency ideally approaching 100% collector/drain efficiency (DE) [1]. The high-efficiency property of the class-E PA stems from the fact that the transistor's voltage and current waveforms are shaped in such a way that they do not overlap each other, and therefore, minimize power dissipation within the transistor. Higher PA efficiency in handset mobile units and in transmitter base stations means smaller size of heat sink, and hence, improved reliability due to reduced thermal dissipation, longer talk time, and less CO_2 emission. Fundamental concepts of the classic class-E PA topology including design equations for calculating circuit component values were extensively explained in [2] and [3].

Manuscript received July 08, 2008; revised November 06, 2008. First published January 09, 2009; current version published February 06, 2009. This work was supported by the U.K. Engineering and Physical Science Research Council (EPSRC) under Grant EP/D020913/1.

The authors are with the Department of Electronic, Electrical and Computer Engineering, University of Birmingham, Edgbaston, Birmingham B15 2TT, U.K. (e-mail: m.thian@bham.ac.uk)

Color versions of one or more of the figures in this paper are available online at http://ieeexplore.ieee.org.

Digital Object Identifier 10.1109/TMTT.2008.2011164

A newly introduced inverse class-E PA proposed in [4] has a number of advantages over the classic class-E PA including 20% lower peak switching voltage, lower inductance values, higher load resistance, inherent absorption of the transistor's output inductances including bond wires, and better scope for optimization for high efficiency at higher output power level, as well as higher peak output power. Unlike the classic class E, which applies zero voltage switching (ZVS) and zero voltage derivative switching (ZVDS) conditions, the inverse class E employs zero current switching (ZCS) and zero current derivative switching (ZCDS) conditions.

Not only high efficiency, but wide bandwidth is also desirable for the PAs, particularly because the present trend of the mobile phone technology moves toward a multiband and multimode system where different wireless communication standards with different frequency band allocations such as global positioning system (GPS), digital enhanced cordless telecommunications (DECT), global system for mobile communications (GSM), Universal Mobile Telecommunications System (UMTS), Bluetooth, and wireless local area network (WLAN) are to be integrated altogether. Techniques for broadband class-E PA designs are treated in [5] and [6].

Present and future generations of mobile communication systems, third generation (3G) and fourth generation (4G), require that RF PAs shall have an excellent linearity performance. A linear output is necessary in order to minimize interferences between different users of the communications system. The more linear the transmitters, the more user channels can be fitted into the available radio spectrum. Different types of linearization such as predistortion [7], feedback and feed-forward system [8], and neural network approach [9] have been developed, but the effectiveness of these linearization schemes are mainly limited by memory effects. Sophisticated predistortion techniques such as Volterra [10], Wiener, Hammerstein [11], and memory polynomials [12] have been proposed to deal with the memory effects. A simpler, yet effective method known as injection was described in [13] where second-harmonic $(2f_1, 2f_2)$ and difference-frequency $(f_1 - f_2, f_2 - f_1)$ injections were applied, and in [14], where third-order signals $(2f_1 - f_2, 2f_2 - f_1)$ were injected to the PA.

In this paper, for the first time, a broadband inverse class-E RF PA with inherent high efficiency is linearized using a combined lookup table (LUT) and improved injection predistortion method. Fundamental principles of the proposed injection together with a new technique to accurately measure the phase of the third-order intermodulation (IM3) will be explained in Section III. The combined technique can achieve significant re-

0018-9480/$25.00 © 2009 IEEE

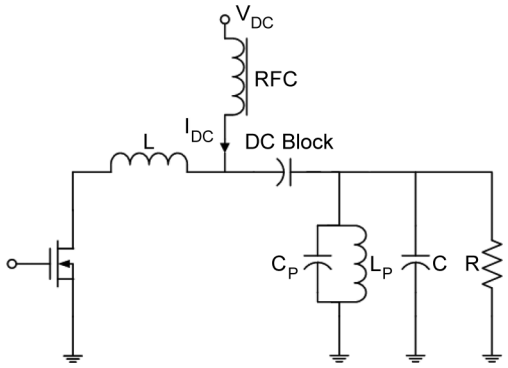

Fig. 1. Inverse class-E PA topology

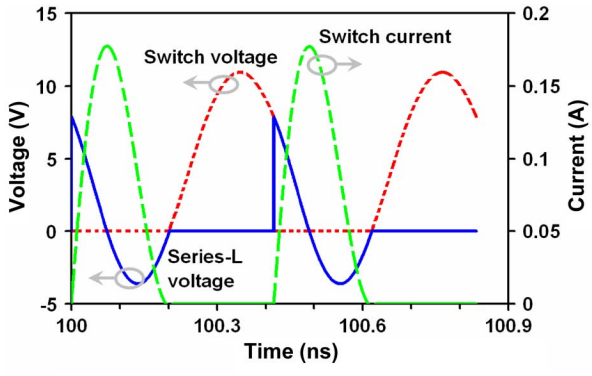

Fig. 2. Simulated current and voltage waveforms of an idealized 0.2-W 4-V 2.4-GHz inverse class-E PA.

ductions of both memory effects and in-band and sideband distortions. The reduction of in-band distortion is demonstrated by a reasonably small value of error vector magnitude (EVM). The technique, therefore, has potential to be utilized in modern wireless communication systems.

II. Inverse Class-E PA Design

A. Theory and Simulation

The basic circuit of the inverse class-E PA is shown in Fig. 1. It is comprised of a transistor, a series inductor (L), a parallel-tuned resonator $(L_P - C_P)$, a shunt capacitor (C), and a load resistance (R). The shunt capacitor C is required in order to compensate for the fundamental-frequency phase shift. The dc current $(I_{\rm DC})$ passing through the RF choke is transformed by transistor on–off switching action into a series of related fundamental-frequency and harmonic currents. The harmonic currents are then filtered out by the high-Q parallel-tuned resonator; hence, leaving only the fundamental-frequency current. For a given combination of output power (Po), dc supply voltage $(V_{\rm DC})$, and operating frequency (f_o where $\omega_o = 2\pi f_o$), optimum circuit component values of the inverse class-E PA are given in [4,Table 1]. Peak switch voltage (V_{SM}) and current (I_{SM}) are computed using [4,eqs. (28) and (30)].

As an example, a 0.2-W 4–V inverse class-E PA operating at 2.4 GHz was designed. A circuit employing an ideal switch model with $R_{\rm ON} = 1$ mΩ and $R_{\rm OFF} = 100$ kΩ and ideal lumped components was simulated within Agilent Technologies' Advanced Design System (ADS) suite. Current and voltage waveforms generated using transient simulations in ADS are shown in Fig. 2. From inspection of Fig. 2, the values of V_{SM} and I_{SM} are, respectively, 11 V and 175 mA, and this agrees well with theoretical prediction dictated in [4, eqs. (28) and (30)]. Further, ZCS and ZCDS conditions as required for an inverse class-E PA operation are satisfactorily met.

B. Implementation and Measurement

The inverse class-E PA depicted in Fig. 3 was constructed using an MwT-8 GaAs MESFET and Rogers RO4003C material with substrate thickness of 813 μm (32 mil), dielectric constant of 3.38, and copper thickness of 35 μm (1 oz). Here, the parallel-tuned resonator $L_P - C_P$ and the shunt capacitor C in Fig. 1 were replaced by two open-circuit stubs whose electrical lengths are 90° at second and third harmonic frequencies in order to suppress the second and third harmonic currents, respectively. The characteristic impedances of these stubs are determined in such a way that the optimum inverse class-E fundamental-frequency load admittance, i.e., $G + j\omega_o C$ (where $G = 1/R$) is met.

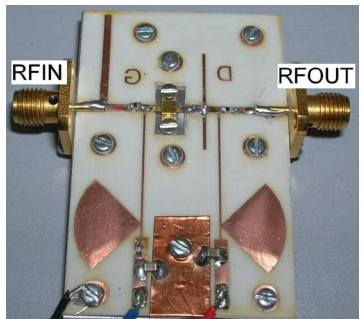

Fig. 3. Constructed inverse class-E PA.

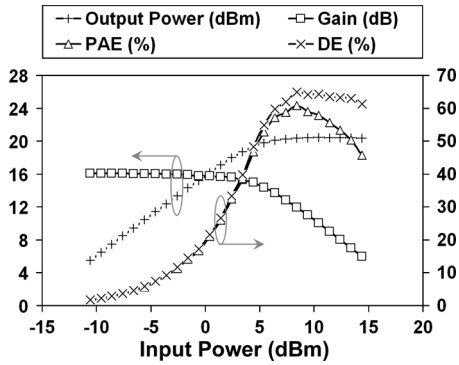

Fig. 4. Measured output power, gain, DE, and PAEs versus RF input power.

Measured (P_o), gain, DE, and power-added efficiency (PAE) versus RF input power are illustrated in Fig. 4. With the transistor biased with $V_{\rm GS} = -2.18$ V and $V_{\rm DC} = 3$ V, a peak DE of 65% and a peak PAE of 61% were obtained at frequency of 2.26 GHz and at an output power of 20.4 dBm. The RF input power applied to the PA was 8.4 dBm, yielding 12-dB gain. The

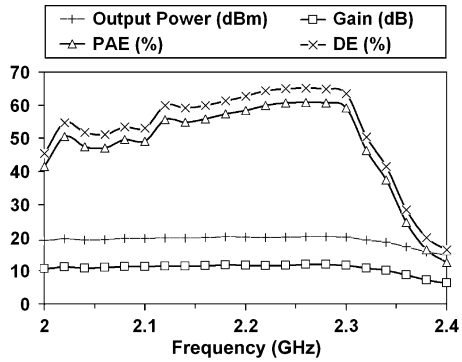

Fig. 5. Measured output power, gain, DE, and PAEs versus frequency.

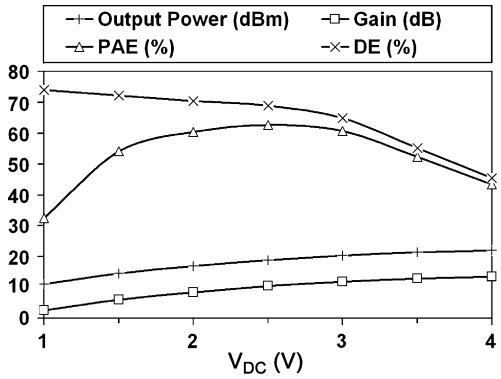

Fig. 6. Measured output power, gain, DE, and PAEs versus dc supply voltage.

measured optimum frequency (2.26 GHz) shifted from the simulated design frequency (2.4 GHz) mainly due to the inaccurate large-signal model of the transistor, as well as fabrication tolerances of the substrate's dielectric constant and surface-mount technology (SMT) passive components.

Fig. 5 presents the plot of measured P_o, gain, DE, and PAE versus frequency for an RF input power of 8.4 dBm. Within a 300-MHz bandwidth from 2.02 to 2.32 GHz, DE of better than 50% and PAE of better than 46% can be obtained with 1-dB output power flatness.

The PA's performance as a function of $V_{\rm DC}$ is shown in Fig. 6. When $V_{\rm DC}$ is varied from 1.5 to 3 V, DE and PAE remain higher than 65% and 54%, respectively, and typical quadratic behavior of output power as a function of $V_{\rm DC}$ is observed as follows:

$$10^{(20.4\ \text{dBm}-14.5\ \text{dBm})/10} \approx (3\ \text{V}/1.5\ \text{V})^2. \tag{1}$$

This feature is, although not further pursued here, required for effective utilization of the inverse class-E PA in envelope elimination and restoration (EER) linearization schemes.

III. New Digital Baseband Predistortion Technique

A. Improved Injection Technique

To obtain good understanding of the proposed injection concept, two-tone carriers are first considered. The output spectrum generated by the vector signal analyzer (VSA) contains information of both amplitude and phase of two carriers (C_1, C_2) at frequencies f_1 and f_2 (where $f_2 > f_1$), as well as lower and upper third-order IMD products (IM3L and IM3U) at frequencies $f_L = 2f_1 - f_2$ and $f_U = 2f_2 - f_1$, respectively,

$$\begin{aligned} v_{\rm OUT} &= C_1 + C_2 + {\rm IM3}L + {\rm IM3}U \\ &= |C_1|e^{j\omega_1 t} + |C_2|e^{j\omega_2 t} + |{\rm IM3}L|e^{j\omega_L t} + |{\rm IM3}U|e^{j\omega_U t} \end{aligned} \tag{2}$$

where

$$\omega_L = 2\pi f_L = 2\omega_1 - \omega_2 \tag{3}$$

$$\omega_U = 2\pi f_U = 2\omega_2 - \omega_1. \tag{4}$$

A key principle of the injection technique in a two-tone scheme is to generate a pair of signals, which cancel both IM3L and IM3U at the output. This implies that such signals must have the same amplitude, but be in antiphase with respect to the original IM3L and IM3U. The problem is while amplitudes of $C_1, C_2,$ IM3L, and IM3U obtained from the VSA are constants their phases change with time, and therefore, a phase reference is critically needed. For example, in [15], a coupler was used to extract a portion of the input signal for use as an IM3 reference to be compared with output signal. In [16], a driving amplifier was utilized to create the IM3 reference, and further in [17], a software-based input signal was generated to define a zero initial phase. In this paper, the IM3 reference is obtained by manipulating phase relationship between output of IM3 and the two carriers.

Correlation between $\omega_L t$ with the phasors of C_1 and C_2 is described by

$$e^{j\omega_L t} = e^{j(2\omega_1 - \omega_2)t} = \frac{C_1^2 C_2^*}{|C_1^2 C_2|}. \tag{5}$$

Consider a case where two carriers and an injected signal $K_L e^{j\Phi_L}$ required for counteracting the lower sideband IM3 are fed to the input of a PA. The total output IM3L will consist of two parts, the first part, IM3L_C, is produced by two carriers and the second one, IM3L_I, is the injected signal $K_L e^{j\Phi_L}$ having been amplified by the PA with a linear gain of $G_{\rm PA\_L}$

$${\rm IM3}L = {\rm IM3}L_C e^{j\omega_L t} + {\rm IM3}L_I e^{j\omega_L t} \tag{6}$$

where

$${\rm IM3}L_I = G_{\rm PA\_L}(K_L e^{j\Phi_L}). \tag{7}$$

Dividing (6) by $e^{j\omega_L t}$ results in

$$\frac{{\rm IM3}L}{e^{j\omega_L t}} = {\rm IM3}L_C + G_{\rm PA\_L}(K_L e^{j\Phi_L}). \tag{8}$$

Using (5), (8) can be rewritten as

$${\rm IM3}L_C + G_{\rm PA\_L}(K_L e^{j\Phi_L}) = {\rm IM3}L\frac{|C_1^2 C_2|}{C_1^2 C_2^*}. \tag{9}$$

Suppose ${\rm IM3}L_C = a + jb$ and $G_{\rm PA\_L} = c + jd$. Here, the gain of the PA is a complex number because of AM/AM and AM/PM characteristics of the PA. To obtain the values of ${\rm IM3}L_C$ and $G_{\rm PA\_L}$, a number of measurements need to be taken from which the complex values of C_1, C_2, and IM3L can be

extracted. For example, if in the first measurement an injection signal with an arbitrary value of $K_L = K_{L1}$ and $\Phi_L = 0°$ is generated and in the second measurement $K_L = K_{L1}$ and $\Phi_L = 180°$, then the values of a, b, c, and d can be determined using (9) from just two measurements. The parameters K_L and Φ_L of the injected signal can then be obtained by setting $\mathrm{IM3}L$, or accordingly, the right-hand side of (9) is equal to $0 + j0$ as follows:

$$(a + jb) + (c + jd)K_L(\cos\Phi_L + j\sin\Phi_L) = 0 + j0 \quad (10)$$

and this results in

$$\Phi_L = \tan^{-1}\left(\frac{bc - ad}{bd + ac}\right) \quad (11)$$

$$K_L = \frac{-a}{c\cos\Phi_L - d\sin\Phi_L}. \quad (12)$$

The same design procedure applies for generating an injected signal required for cancelling the output $\mathrm{IM3}U$. A problem appears when two carriers (C_1, C_2) together with lower and upper sideband injected signals $(\mathrm{IM3}L_I, \mathrm{IM3}U_I)$ are simultaneously generated and fed to the PA. Interaction between the carriers C_1 and C_2, and the injected signal $K_L e^{j\Phi_L}$ will affect the output $\mathrm{IM3}U$ and similarly interaction between C_1 and C_2, and the injected $K_U e^{j\Phi_U}$ will affect the output $\mathrm{IM3}L$, as described in

$$\omega_L = \omega_1 + \omega_2 - \omega_U \quad (13)$$

$$\omega_U = \omega_1 + \omega_2 - \omega_L. \quad (14)$$

Taking into account the contribution of this interaction to the output $\mathrm{IM3}L$, (8) is modified into

$$\begin{aligned}\mathrm{IM3}L &= \mathrm{IM3}L_C e^{j\omega_L t} + G_{\mathrm{PA\_}L}(K_L e^{j\Phi_L})e^{j\omega_L t} \\ &\quad + \alpha_{U\_L} e^{j\omega_1 t} e^{j\omega_2 t}(K_U e^{j\Phi_U} e^{j\omega_U t})^* \\ &= \left\{\mathrm{IM3}L_C + G_{\mathrm{PA\_}L}(K_L e^{j\Phi_L}) \right. \\ &\quad \left. + \alpha_{U\_L} K_U e^{-j\Phi_U}\right\} e^{j\omega_L t} \end{aligned} \quad (15)$$

and similarly, the output $\mathrm{IM3}U$ becomes

$$\begin{aligned}\mathrm{IM3}U = \left\{\mathrm{IM3}U_C + G_{\mathrm{PA\_}U}(K_U e^{j\Phi_U}) \right. \\ \left. + \alpha_{L\_U} K_L e^{-j\Phi_L}\right\} e^{j\omega_U t}\end{aligned} \quad (16)$$

where α_{U_L} is a constant, which represents the contribution of the interaction of C_1 and C_2 and the injected signal $K_U e^{j\Phi_U}$ to the output $\mathrm{IM3}L$, and α_{L_U} is a constant, which represents the contribution of the interaction of C_1 and C_2, and the injected signal $K_L e^{j\Phi_L}$ to the output $\mathrm{IM3}U$. By setting $\mathrm{IM3}L$ and $\mathrm{IM3}U$ in (15) and (16) equal to 0, we can obtain a solution for dual sideband predistortion as follows:

$$\begin{bmatrix} K_L e^{j\Phi_L} \\ K_U e^{-j\Phi_U} \end{bmatrix} = -\begin{bmatrix} G_{\mathrm{PA\_}L} & \alpha_{U\_L} \\ \alpha^*_{L\_U} & G^*_{\mathrm{PA\_}U} \end{bmatrix}^{-1} \begin{bmatrix} \mathrm{IM3}L_C \\ \mathrm{IM3}U^*_C \end{bmatrix}. \quad (17)$$

Note that $*$ in (15) and (17) denotes complex conjugate. If $Z_1 = aZ_2 e^{j\alpha} + bZ_3 e^{j\beta}$, then the complex conjugate of Z_1, i.e., Z_1^*, will be $aZ_2^* e^{-j\alpha} + bZ_3^* e^{-j\beta}$, where Z_1, Z_2, and Z_3 are complex numbers and a and b are real numbers.

In [18], a graphical method to determine the correct phase for the IM3 injected signals was proposed since the available spectrum analyzer did not provide phase information. However, the method did not take into account the interactions described above, between the two carriers and the injected IM3 signals. As a consequence, the philosophy behind the concept described in [18] needs to be extended since it could lead to serious convergence problems, particularly when α_{U_L} and α_{L_U} are high.

B. Combined Injection and LUT Techniques

The concept of the proposed injection technique has earlier been explained for two-tone signals. When applying this injection to a wideband modulated signal such as 16 quadrature amplitude modulation (QAM) or CDMA, two brick walls, i.e., one for the lower sideband and the other for the upper sideband, are introduced. Each brick wall is comprised of a number of sub-frequency components, which can be analogously considered as multitone signals, and therefore, an elaboration of the concept explained in Section III-A where two-tone signals were considered can be applied directly. As expected, due to the interactions among sub-frequency components, the size of the matrix in (17) is increased. For example, if each sideband is divided into 50 sub-frequency components, then the solution for $K_i e^{j\Phi_i}$ where $i = 1, 2, 3, \ldots, N$ and $N = 100$ will involve a 100×100 matrix, and therefore, is not practical.

To cope with this problem, an alternative iterative computational method, as described in the flowchart in Fig. 7, can be used. Two measurements (with input phase $\Phi = 0°$ and $180°$) are required for each sub-frequency component. The correct amplitude and phase of the injected signal can be computed using (11) and (12). If, at a certain sub-frequency, the interaction between the carrier and an injected signal has a substantial effect on the output IMD products at other sub-frequencies, then the algorithm in Fig. 7 suggests a reduction of K_i (e.g., by a factor of 2) in order to minimize the resulting error in the computed phase (11). This error is further reduced in subsequent iterations. Since the nonlinearity is lower after the first injection, in the second iteration, the initial value of K_i, i.e., α, is reduced (e.g., by a factor of 10). The iteration is terminated once the goal has been achieved. Reducing the IMD products to the noise floor of the equipment is typically set as the ultimate goal. The final injected signal at a certain sub-frequency is the vector sum of the injected phasors resulting from each iteration.

The experimental setup for the linearization of the inverse class-E PA is illustrated in Fig. 8. A PC generates both the digital baseband signals and the injected signals and then passes them to an I/Q modulator generator (AMIQ). I and Q analog signals generated by the AMIQ are modulated and up-converted to RF frequencies by a signal generator with a built-in modulator (SMIQ). The modulated signal is then fed to the inverse class-E PA operated near saturation and the resulting output signal is down-converted and demodulated to baseband I and Q signals and sampled inside a VSA.

Fig. 9 shows AM/AM and AM/PM conversion of the fabricated inverse class-E PA. The nonlinearity of the measured AM/PM when compared to the measured AM/AM appears more significant with large phase variations of up to 18°. The

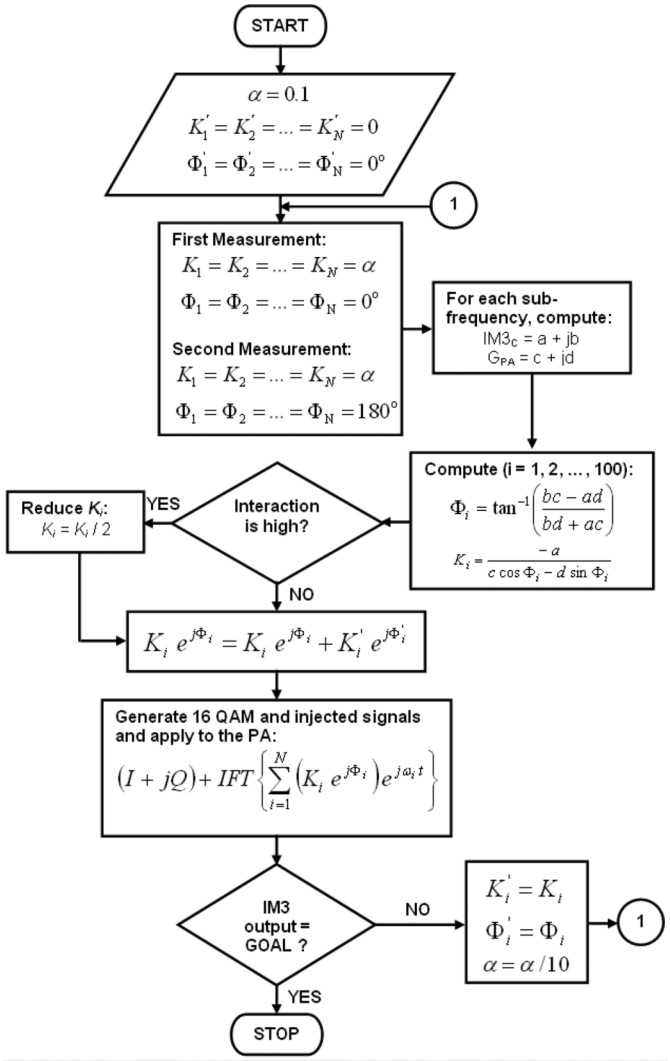

Fig. 7. Flowchart for iterative computation of the improved injection technique. IFT stands for inverse Fourier transform.

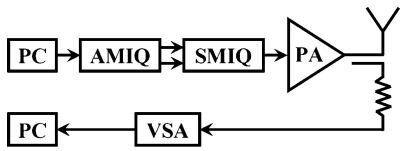

Fig. 8. Experimental setup for linearization.

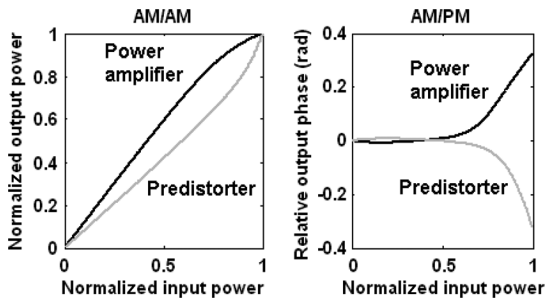

Fig. 9. Normalized AM/AM and AM/PM measurement results.

fundamental principle of LUT predistortion is to create inverse characteristics of the AM/AM and AM/PM (Fig. 9) so that the combined predistorter and PA will result in a linear operation.

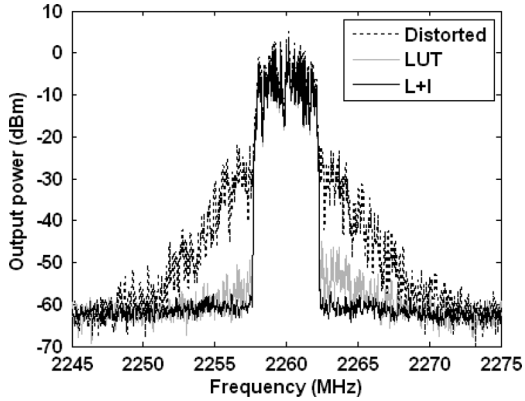

Fig. 10. Comparison of measured output spectrum: distorted, LUT, and $L + I$ signals.

The measured output spectrum of the inverse class-E PA operated near the saturation for a 16-QAM modulated signal with 5.6-dB peak-to-average ratio (PAR) is depicted in Fig. 10. Spectral regrowth observed in Fig. 10 indicates that the PA was driven sufficiently hard. Also shown in Fig. 10 is the output spectrum when a LUT predistorter is employed. It can be seen that the sideband distortion can be partially reduced. Amplitude asymmetry between the lower and upper sideband is also observed and it is due to memory effects [19].

A combined LUT and injection predistortion technique $(L + I)$ is proposed here. The LUT is first applied to reduce the degree of the nonlinearities of the PA, particularly because it can handle in-band distortion well, while the injection cannot. The injection scheme can then be subsequently applied to the PA not only to further suppress the IMD down to the noise floor, but particularly to minimize the memory effects due to its unique capability that the LUT does not have, i.e., to selectively control the sub-frequency sideband components. Fig. 10 shows the output spectrum of the combined $L + I$ technique where neither spectral regrowth, nor memory effects are present any longer. It can also be observed from Fig. 10 that the proposed $L+I$ predistortion technique results in approximately 34-dB adjacent channel leakage power ratio (ACLR) improvement. Since the nonlinearities of the PA had been reduced by first applying the LUT, only one iteration was needed for the injection, and therefore, it was faster because fewer measurements were taken.

The PAR values of the measured output signal with and without predistorter are 5.7 and 5.1 dB, respectively. Measured EVMs (rms) of the distorted, LUT, and $L+I$ output signals are, respectively, 6.9%, 0.8%, and 0.7%, where the last two satisfy the requirements for modern wireless communication systems, such as WLAN 802.11, WiMAX 802.16, and 3G (WCDMA, CDMA2000).

IV. Conclusion

Linearization of a highly efficient broadband inverse class-E PA using a combined LUT and enhanced injection technique has been demonstrated. Without a predistorter, significant spectral regrowth was observed when a nonconstant envelope 16-QAM signal was applied to the PA since the PA was driven hard. The proposed linearization technique has been shown to be able to

facilitate effective reduction of both in-band and sideband distortion, and more importantly, can cope well with memory effects. An ACLR improvement of approximately 34 dB was obtained with 0.7% measured EVM (rms).

ACKNOWLEDGMENT

The authors would like to thank MicroWave Technology Inc. and Prof. V. Fusco for the MESFETs, Dr. F. Raab and Dr. A. Grebennikov for fruitful correspondences, and A. Yates and A. Zentani for helping in the board's fabrication.

REFERENCES

[1] N. O. Sokal and A. D. Sokal, "Class-E—A new class of high-efficiency tuned single ended switching power amplifiers," *IEEE J. Solid-State Circuits*, vol. SSC-10, no. 3, pp. 168–176, Jun. 1975.

[2] F. H. Raab, "Idealized operation of the class-E tuned power amplifier," *IEEE Trans. Circuits Syst.*, vol. CAS-24, no. 12, pp. 725–735, Dec. 1977.

[3] A. Grebennikov and N. O. Sokal, *Switchmode RF Power Amplifiers*. Oxford, U.K.: Elsevier, 2007.

[4] T. Mury and V. F. Fusco, "Series-L/parallel-tuned comparison with shunt-C/series-tuned class-E power amplifier," *Proc. Inst. Elect. Eng.—Circuits Devices Syst.*, vol. 152, no. 6, pp. 709–717, Dec. 2005.

[5] N. Kumar, C. Prakash, A. Grebennikov, and A. Mediano, "High-efficiency broadband parallel-circuit class E RF power amplifier with reactance-compensation technique," *IEEE Trans. Microw. Theory Tech.*, vol. 56, no. 3, pp. 604–612, Mar. 2008.

[6] J. K. A. Everard and A. J. King, "Broadband power efficient class E amplifiers with a non-linear CAD model of the active MOS device," *J. Inst. Electron. Radio Eng.*, vol. 57, pp. 52–58, Mar. 1987.

[7] W. Woo, M. D. Miller, and J. S. Kenney, "A hybrid digital/RF envelope predistortion linearization system for power amplifiers," *IEEE Trans. Microw. Theory Tech.*, vol. 53, no. 1, pp. 229–237, Jan. 2005.

[8] P. B. Kenington, *High-Linearity RF Amplifier Design*. Norwood, MA: Artech House, 2000.

[9] K. C. Lee and P. Gardner, "Adaptive neuro-fuzzy inference system (ANFIS) digital predistorter for RF power amplifier linearization," *IEEE Trans. Veh. Technol.*, vol. 55, no. 1, pp. 43–51, Jan. 2006.

[10] C. Eun and E. J. Powers, "A new Volterra predistorter based on the indirect learning architecture," *IEEE Trans. Signal Process.*, vol. 45, no. 1, pp. 223–227, Jan. 1997.

[11] L. Ding, R. Raich, and G. T. Zhou, "A Hammerstein predistortion linearization design based on the indirect learning architecture," in *IEEE Int. Acoust., Speech, Signal Process. Conf.*, Orlando, FL, May 2002, vol. 3, pp. 2689–2692.

[12] D. R. Morgan, Z. X. Ma, J. Kim, M. G. Zierdt, and J. Pastalan, "A generalized memory polynomial model for digital predistortion of RF power amplifiers," *IEEE Trans. Signal Process.*, vol. 54, no. 10, pp. 3852–3860, Oct. 2006.

[13] C. S. Aitchison, M. Mbabele, M. R. Moazzam, D. Budimir, and F. Ali, "Improvement of third-order intermodulation product of RF and microwave amplifiers by injection," *IEEE Trans. Microw. Theory Tech.*, vol. 49, no. 6, pp. 1148–1154, Jun. 2001.

[14] K. J. Cho, D. H. Jang, S. H. Kim, J. Y. Kim, J. H. Kim, and S. P. Stapleton, "An analog compensation method for asymmetric IMD characteristics of power amplifier," *IEEE Microw. Wireless Compon. Lett.*, vol. 14, no. 4, pp. 153–155, Apr. 2004.

[15] J. C. Pedro and J. P. Martins, "Amplitude and phase characterization of nonlinear mixing products," *IEEE Trans. Microw. Theory Tech.*, vol. 54, no. 8, pp. 3237–3245, Aug. 2006.

[16] S. Y. Lee, Y. S. Lee, and Y. H. Jeong, "A novel phase measurement technique for IM3 components in RF power amplifiers," *IEEE Trans. Microw. Theory Tech.*, vol. 54, no. 1, pp. 451–457, Jan. 2006.

[17] C. Crespo-Cadenas, J. Reina-Tosina, and M. J. Madero-Ayora, "Phase characterization of two-tone intermodulation distortion," in *IEEE MTT-S Int. Microw. Symp. Dig.*, Long Beach, CA, Jun. 2005, pp. 1505–1508.

[18] D. Rabijns, W. Van Moer, and G. Vandersteen, "Spectrally pure excitation signals: Only a dream?," *IEEE Trans. Instrum. Meas.*, vol. 53, no. 5, pp. 1433–1440, Oct. 2004.

[19] J. S. Kenney and P. Fedorenko, "Identification of RF power amplifier memory effect origins using third-order intermodulation distortion amplitude and phase asymmetry," in *IEEE MTT-S Int. Microw. Symp. Dig.*, San Francisco, CA, Jun. 2006, pp. 1121–1124.

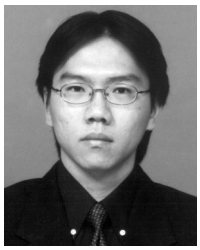

Mury Thian received the B.Sc. degree in electronics from Atma Jaya University, Jakarta, Indonesia, in 2001, the M.Sc. degree in microelectronics from Delft University of Technology, Delft, Netherlands, in 2004, and the Ph.D. degree in microwave electronics from Queen's University Belfast, Belfast, U.K., in 2007.

From 2003 to 2004, he gained industrial experience with Philips Semiconductors (now NXP), Nijmegen, The Netherlands. In 2008, he joined the University of Birmingham, Birmingham, Edgbaston, U.K., as a Research Fellow. His research interests include RF integrated circuit (RFIC)/monolithic microwave integrated circuit (MMIC) design, micropower circuits design, emerging device technology, efficiency enhancement, and linearization techniques for PAs.

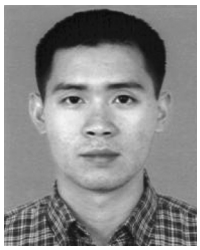

Ming Xiao (S'08) was born in Guangzhou, China, in 1983. He received both the B.Sc. degree in electronic engineering from Fudan University, Shanghai, China, and the B.Eng. degree (first-class Hons.) in electronic and computer engineering from the University of Birmingham, Birmingham, Edgbaston, U.K. in 2005 (double degrees), and is currently working toward the Ph.D. degree in electronic and electrical engineering at the University of Birmingham.

His general research interests are in the areas of microwave amplifier linearization techniques, signal processing, and artificial intelligence.

Peter Gardner (M'98–SM'00) received the B.A. degree in physics from the University of Oxford, Oxford, U.K., in 1980, and the M.Sc. and Ph.D. degrees in electronic engineering from The University of Manchester Institute of Science and Technology (UMIST), Manchester, U.K., in 1990 and 1992, respectively.

From 1981 to 1987, he was with Ferranti, Poynton, Cheshire, U.K., as a Senior Engineer in microwave amplifier development. From 1987 to 1989, he worked freelance in microwave engineering and software. In 1989, he joined the Department of Electrical Engineering and Electronics, UMIST, as a Research Associate, where he carried out research in microwave negative resistance circuits, low-noise MMIC design, and tunable planar resonators. In 1994, he became a Lecturer with the Department of Electronic, Electrical, and Computer Engineering, University of Birmingham, Birmingham, Edgbaston, U.K., and became a Senior Lecturer in 2002. His current research interests are in the areas of microwave and millimetric integrated active antennas and beamformers, cognitive radio, and microwave amplifier linearization techniques.